Porosity as a Design Element for Developing Catalytic Molecular Materials for Electrochemical and Photochemical Carbon Dioxide Reduction

*Patricia De La Torre, Lun An, and Christopher J. Chang**

P. De La Torre, Dr. L. An, Prof. C. J. Chang

Department of Chemistry, University of California, Berkeley

94720-1460 Berkeley, CA (USA)

and

Chemical Sciences Division, Lawrence Berkeley National Laboratory

94720-1460 Berkeley, CA (USA)

E-mail: chrischang@berkeley.edu

Prof. C. J. Chang

Department of Molecular and Cell Biology, University of California, Berkeley

94720-1460 Berkeley, CA (USA)

Keywords: carbon dioxide reduction, porosity, molecular materials, catalysis

Abstract: The catalytic reduction of carbon dioxide (CO_2) using sustainable energy inputs is a promising strategy for upcycling of atmospheric carbon into value-added chemical products. This goal has inspired the development of catalysts for selective and efficient CO_2 conversion using electrochemical and photochemical methods. Among the diverse array of catalyst systems designed for this purpose, two- and three-dimensional platforms that feature porosity offer the potential to combine carbon capture and conversion. Included are covalent organic frameworks (COFs), metal-organic frameworks (MOFs), porous molecular cages, and other hybrid molecular materials developed to increase active site exposure, stability, and water compatibility while maintaining precise molecular tunability. This mini-review showcases catalysts for the CO_2 reduction reaction (CO_2RR) that incorporate well-defined molecular elements integrated into porous materials structures. Selected examples provide insights into how different approaches to this overall design strategy can augment their electrocatalytic and/or photocatalytic CO_2 reduction activity.

1. Introduction

The world population's dependence on finite natural resources for energy storage and generation can be mitigated by replacement with renewable and sustainable sources such as electricity from wind, solar, and hydropower.[1] Efforts to decarbonize our current and future energy infrastructure are critical to addressing detrimental effects of petroleum combustion manifesting as rising global temperatures, ocean acidification, and increased frequency of extreme weather events.[2] Many of these phenomena can be attributed to rising concentrations of atmospheric CO_2, now peaking at 421 ppm in 2022; this situation demands restoration of the carbon cycle to its natural balance as an important step in a zero-emissions future.[3] One approach under current investigation is the direct air capture of CO_2 and its subsequent transformation into value-added products via the CO_2 reduction reaction (CO_2RR). CO_2 reduction via multi-electron, multi-proton transfer reaction processes can effectively store sustainable energy in the form of chemical bonds.[2b, 4]

Although CO_2RR is a promising strategy to store energy derived from clean and renewable sources and simultaneously mitigate climate change, it is thermodynamically costly to activate the linear and symmetric CO_2 molecule by a single electron transfer due to the large reorganization energy associated with producing the bent radical anion (–1.9 V vs NHE).[5] With the inclusion of multiple protons and electrons, CO_2 reduction can be achieved at more moderate potentials. However, this multielectron, multiproton chemistry comes at the cost of product selectivity; within a relatively narrow potential window (–0.24 to –0.61 V), a variety of carbon products such as CO, HCOOH, HCHO, CH_3OH, and CH_4 can theoretically be formed, but in most cases the reduction of protons to hydrogen in the hydrogen evolution reaction (HER) is facile (0 V) and dominant over carbon-based product formation. As such, developing catalyst platforms capable of efficient and selective CO_2RR presents one attractive avenue in solving these challenges. Moreover, applying electrochemistry and/or photochemistry as sustainable energy inputs that drive the electron transfer processes for CO_2RR can guide the optimization of these platforms.[4a] In terms of efficiency, CO_2RR electrocatalysts require close energy matching between their onset potential and the thermodynamic potential required for the desired CO_2 transformation in order to minimize the excess energy required to drive the reaction (i.e., overpotential). Performance metrics such as Faradaic efficiency (FE) and current density further describe the catalyst activity relative to the electron transfer productivity and stability from electrode to catalyst. In photocatalytic CO_2RR systems, efficiency is in turn affected by photosensitization, which can be achieved by the catalyst itself if it has productive light absorption, or by a separate photosensitizer with a matched excited state energy (analogous to overpotential).[6] Additionally, sacrificial electron donors are needed to regenerate the active photosensitizer. Performance metrics such as the turnover number (TON) and the quantum yield (QY) for product formation quantify the photocatalyst activity in terms of stability and productive photon absorption (analogous to FE). Along these lines, achieving the delicate balance between low overpotentials, high turnover frequencies (TOF), FE,QY, and the suppression of the HER in the presence of aqueous media is essential for effective catalyst performance.

Against this backdrop, the development of homogeneous catalysts offers a valuable starting point towards fundamental understanding of CO_2 activation and reduction mechanisms, where molecular

complexes bearing precise chemical structures can be tuned via metal substitutions, ligand variations, and secondary coordination sphere modifications.[4a, 5, 7] In contrast, heterogeneous materials present greater challenges in defining active sites and reaction intermediates, but are often more water compatible and achieve higher activities and longer life cycles compared to homogenous congeners.[4d, 4e, 8] As such, bridging the interface between molecularly precise homogeneous catalysts and polymorphous yet robust heterogeneous material catalysts, in an area termed molecular materials, offers the possibility to draw from the best attributes of both worlds.[7g, 7i, 9] Indeed, molecular materials designed to mirror aspects of both homogeneous and heterogeneous catalysts can produce highly stable, crystalline systems with molecular modularity.

In this context, a unifying feature of an important class of molecular materials, which span covalent organic frameworks (COFs), metal-organic frameworks (MOFs), and porous molecular cages, is the construction of porosity from precise geometric connection of molecular building blocks (Figure 1). In terms of biology-to-chemistry concept transfer for designing CO_2RR catalysts, porous molecular materials can serve as functional synthetic models for biological enzyme-substrate dynamics by providing a confined space microenvironment to target increased CO_2 substrate diffusion and activation for efficient conversion into value-added chemical products.[4f] In this mini-review, we highlight major classes of porous molecular materials structures for electrochemical and/or photochemical CO_2RR, including MOFs, COFs, porous molecular cages, and hybrid molecular materials. Rather than provide a comprehensive compilation of structures, we focus on select examples to showcase key design elements to achieving stable and active CO_2RR catalysis, including **mass transport, charge transfer, light absorption, activating groups, and electrode construction** (Figure 1).

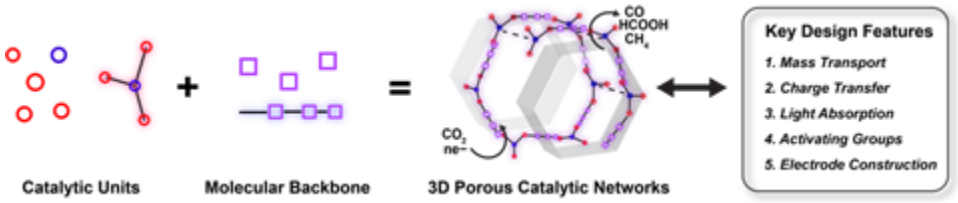

Figure 1. Conceptual design schematic of porous molecular materials catalysts for the carbon dioxide reduction reaction (CO_2RR), comprised of discrete molecular units combining to form functional porous materials with higher-order dimensions.

2. Key Design Features to Achieving Effective CO_2 Reduction Catalyzed by Porous Molecular Materials

Effective catalysts for CO_2RR using porous molecular materials must meet several criteria, including high selectivity for reduction of the CO_2 substrate over competing proton substrate to avoid the off-target hydrogen evolution reaction (HER), particularly in water, as well as suitable turnover frequencies to match electron and/or solar flux of the sustainable energy input and long-term stability. Porous structures provide a host of key design features that can be used to augment CO_2RR reactivity. First and foremost is **mass transport**, as porous structures enable higher surface areas for diffusion and capture of substrate and/or release of products relative to non-porous analogs. Porosity also benefits **charge transfer**, particularly in electrochemical CO_2RR platforms where site isolation can increase the percentage of electrochemically active sites available for catalysis by alleviating steric blocking between electrode materials and molecular redox units and between molecular units themselves, as well as extending charge transfer beyond the molecule into an extended materials structure in two or three dimensions. **Light absorption** is another element that can be improved by porosity, particularly in two main ways. The first benefit is in site isolation of chromophores, enabling the properties of molecular light-harvesting entities to be translated more directly into materials frameworks. Second, porosity also enables precise placements of donor-acceptor pairs in defined electron-transfer pathways, without direct contact between these components. The confined space environments also provide a modular approach for introduction of **activating groups** to increase CO_2 capture and orient substrate binding and activation, stabilize

CO_2RR intermediates, and/or release value-added products through careful tuning of the secondary coordination sphere. Finally, in terms of electrochemical or photoelectrochemical CO_2RR, porosity can enhance **electrode construction**, where higher surface areas give more sites in the same three-dimensional volume. We now provide a select set of examples of porous molecular materials, grouped by type, that showcase these design features to augment electrochemical and/or photochemical CO_2RR chemistry. As such, a wide range of other design concepts and strategies to constructing selective and efficient CO_2RR catalysts have been reviewed previously and should be explored for a more extensive understanding of this field.[9b, 9d, 10]

3. Covalent Organic Frameworks (COFs)

Reticular chemistry transforms discrete molecular building blocks into extended material scaffolds by linking them in deliberate spatial orientations that result in predictable periodic structures;[11] such reticular materials can retain permanent porosity with molecular-level control of structure. Covalent organic frameworks (COFs) represent one important family of reticular crystalline solids whose molecular units are composed of functional organic ligands.[9a, 11a, 12] Such molecular materials have been developed for applications spanning gas storage and separation, optoelectronics, drug delivery and catalysis.[9a, 13] The COF examples for CO_2RR highlighted in this section outline how the principles of homogeneous molecular catalyst design, such as electronic conjugation, inner and outer-sphere activating groups, merge with porosity and electrode construction in an attempt to create robust CO_2RR materials with tunable reactivity.

3.1. Tunable Porosity and Electronics Enhance CO_2RR in Porphyrin-based COFs

Privileged molecular scaffolds such as porphyrin and phthalocyanine metal complexes have been studied extensively for electrochemical and photochemical catalytic CO_2 reduction.[6, 7b, 7f, 14] An atomic level understanding of how these catalysts operate makes them ideal candidates for incorporation into COF structures,[13f, 15] thus permitting the exploration of molecular properties extrinsic to the CO_2 binding and activation site.

Our laboratory, in collaboration with Yaghi group, reported the first examples of electrochemical CO_2RR in porous structures using COF catalysts as a prototype reticular molecular material.[16] We selected metalloporphyrins as functional COF building units and constructed COF-366-M and COF-367-M (M= Co, Cu) catalysts from the condensation of amine functionalized metalloporphyrin nodes with aldehyde-functionalized phenyl linker struts (Figure 2a). The sizes of the porous cavities were predictably modified by using either mono or biphenyl linkers between the cobalt porphyrin catalytic units, resulting in a 3 Å difference between COF-366-Co and COF-367-Co. With its larger pore size, COF-367-Co achieved a 2-fold and 5-fold enhancement in catalytic efficiency for conversion of CO_2 to CO relative to its COF-366-Co and Co-TAP monomer counterparts, respectively (Figure 2b), which was attributed to higher surface area and an increase in accessible electrochemically active centers from 4 to 8%. Faradaic efficiencies (FEs) for selective CO production reached 91%, even in neutral pH aqueous solvent. Beyond these molecular-level modifications, complementary materials modifications could synergistically improve the performance of these COF platforms as CO_2RR catalysts. In one key advance, the relatively low percentage of observed electroactive centers in first-generation COF CO_2RR catalysts inspired the **electrode construction** that could achieve better electrical contact with the catalytic COF material. For example, moving from deposition of the COF powder to growing oriented thin films of the COF directly onto the electrode surface resulted in improved current density for CO_2-to-CO conversion from 5 to 45 mA/mg and turnover frequencies (TOFs) rising from 98 to 665 h^{-1} for COF-366-Co, with total turnover numbers (TONs) reaching 3,542. The same electrode construction was utilized in a follow-up study, where electron withdrawing groups incorporated at the phenyl linkers established reticular tuning as a design principle for improving CO_2 reduction activity.[17] Indeed, substituting the phenyl linkers in a COF-366-Co platform with the **activating groups** $–(OMe)_2$, –F, and $–(F)_4$ resulted in molecularly precise tuning of reduction potentials and current densities in the functional heterogeneous material (Figure 2a, c).

3.2. Enhancing Charge Transfer in Porphyrin-Based COF CO_2RR Catalysts

Porphyrin molecules are intrinsically highly conjugated compounds. When integrated into a COF structure, this molecular conjugation can extend in multiple dimensions, giving rise to unique electron transfer properties in the resulting materials that can be exploited for electrocatalysis. For example, the use of tetrathiafulvalene (TTF) as a linker in metalloporphyrin-based COFs establishes a catalyst framework with high **charge transfer** mobility. This approach offers a design strategy to improve traditional COF electrodes, which often possess limited conductivity. Indeed, Lan and co-workers reported that in Co-TTCOF, the TTF linkers enable rapid charge transfer from the electrode to catalytic Co centers,[18] and Co-TTCOF converts CO_2 into CO with a FE of 91.3% at −0.7 V vs RHE at a rate of 1.28 s^{-1}. Moreover, exfoliation of this COF leads to the formation of Co-TTCOF nanosheets (~5 nm in thickness) with an improved FE of 99.7% at −0.8 V, which is attributed to its higher surface area and more accessible active sites from this new **electrode construction.** Exfoliation was also applied as a method to enhance CO_2-to-CH_4 activity in another porphyrin-based COF electrocatalyst.[19]

3.3. Increasing Accessible Active Sites by Expanding COFs from 2D to 3D Materials

The COF-366-Co and Co-TTCOF examples showcase the importance of **electrode construction** in optimizing active site utilization in 2D COF structures for CO_2RR. A complementary approach is to change the materials dimension of the catalyst itself. In this context, although more difficult to design and synthesize compared to their 2D counterparts, 3D COFs offer an attractive family of alternative platform materials for creating frameworks with intrinsic porosity that can achieve larger surface areas and pore diameters for improved CO_2 uptake via **mass transport**.[20] In one example of CO_2RR using a 3D COF, 3D-Por(Co/H)-COF,[20b] demonstrated a FE of 92% for CO production, compared to 82% for COF-366-Co under similar conditions, where both electrodes were constructed from deposition of a COF catalyst ink onto a carbon electrode. The observed improvement in FE for CO_2RR was attributed to a higher number of exposed active sites in the 3D porous COF relative to its 2D congener. In a recent study, Fang and coworkers reported the 3D photocatalyst series, JUC-640-M (M= H, Ni, Co).[21] This unique stp-topologized COF combined triptycene and porphyrin building units resulting in a low-density, ultra-porous structure achieving efficient **mass transport**. This was

reflected in the Co derivative, JUC-640-Co, which showed unprecedented CO_2-to-CO production rates of 15 mmol $g^{-1}h^{-1}$ in conjunction with $[Ru(bpy)_3]^{2+}$ as a photosensitizer and BIH as a sacrificial electron donor.

3.4. Secondary Coordination Sphere Modifications of COF Structures to Improve CO_2RR Performance

In addition to augmenting charge transfer and dimensionality of molecular materials, secondary coordination sphere approaches can be employed to improve catalytic performance of COF systems for CO_2RR. For example, the use of pendant amines as **activating groups** that can form adducts with CO_2 can improve substrate capture for subsequent substrate conversion. Indeed, amines are commonly used as additives in CO_2 capture and conversion, forming carbamate structures.[22] Not only can amines within a COF structure help capture CO_2, but they can also impart high stability for such adducts under harsh catalytic conditions. Specifically, post-synthetic solid-state reduction of a 3D COF (COF-300) or 2D COF (COF-366-M) bearing imine linkages can form the amine-linked analogs COF-300-AR and COF-366-M-AR, respectively.[23] These frameworks persist even after immersion in 6 M HCl and NaOH aqueous solutions for over 12 hours. Further, the addition of COF-300-AR material showed improved FE for CO_2 reduction to CO over a bare Ag electrode (43 vs 83% at –0.85 V vs RHE) under similar conditions. Enhancement in CO_2 uptake and subsequent improvement in reactivity was observed *in situ* in other COF systems, which may be attributed to the reduction of imine linkages by H_2 generated at the start of the photolysis.[24] Finally, the introduction of charged functionalities as **activating groups** has also proven successful in enhancing CO_2RR activity in COF structures. In a recent example, Co-iBFBim-COF-X (X=F^-, Cl^-, Br^-, and I^-),[25] incorporates charged imidazolium groups with variable anions to enhance the stabilization of CO_2 reduction intermediates through hydrogen bonding (Figure 2d). Compared to a neutral analog, Co-iBFBim-COF-I^- displayed 3.5-fold increase in turnover frequency for the production of CO.

3.5. Phthalocyanine based COFs

Cobalt phthalocyanine (CoPc) is another privileged molecular catalyst complex amenable to incorporation into COFs for CO_2RR.[26] Similar to porphyrin analogs, CoPc-based COFs target improved **charge transfer** from electrodes via conjugation of the linkers with its structure. In one example, connecting CoPC in both x and y directions with phenazine linkages creates a highly conjugated 2D COF with tetragonal topology (Figure 1e).[26a] The metal phthalocyanine units have pore channels created by 2.2 nm distance between CoPc units. High chemical stability of CoPc-PDQ-COF was recorded under various organic solvents as well as highly acidic/basic aqueous electrolytes between 25 to 100 ºC. Additionally, CoPc-PDQ-COF was stable over a wide range of applied potentials (−0.32 to −0.66 V). In comparison to the CoPc molecular analog, the PDQ-COF material displayed a 32-fold higher TOF at a 560 mV overpotential. More recently, CoPc-derived COFs were used to compare catalytic activities of 2D versus 3D frameworks. A 3D CoPc polyimide COF with tetraaminophenyl adamantine linkers (Figure 2f), CoPc-PI-COF-3,[26c] possesses 33% electroactive sites compared to only 5% for its 2D analog.[26b] This improvement in electroactive sites and **mass transport** resulted in a 1.5-fold higher current density for CO_2-to-CO conversion (Figure 2g).

3.6. COFs Bearing Metal-Bipyridine Catalytic Units

In addition to porphyrin-based and phthalocyanine-based COFs, another type of privileged catalytic unit for COF-mediated CO_2RR is based on metal-bipyridine complexes, where active sites are incorporated onto a bipyridine-based ligand strut. In this regard, rhenium tricarbonyl complexes of the type $[Re(bpy)(CO)_3Cl]$ are canonical examples of molecular CO_2RR catalysts. Interestingly, these molecular complexes are known to suffer from catalyst degradation pathways involving dimerization of individual Re units to form inactive dimers.[27] Indeed, efforts to address this deactivation pathway in homogeneous solution include the introduction of large alkyl groups proximal to the metal center to sterically encumber the open coordination site under catalytic conditions to prevent the deactivation pathway.[28] A complementary materials approach to prevent this type of deactivation is to immobilize $[Re(bpy)(CO)_3Cl]$ within a COF structure for site isolation. Despite the reasonable nature of this approach, $[Re(bpy)(CO)_3Cl]$ COFs reported to date show only low electrocatalytic[29] and photocatalytic[30] performance for CO_2RR. In one example, a conjugated triazine COF containing

[Re(bpy)$(CO)_3$Cl] active sites (denoted Re-COF) was designed for self-sensitized CO_2RR using visible light irradiation in organic solvent, showing how **light absorption** can be optimized .[30a] After a 20-hour reaction period, Re-COF exhibits a total turnover number (TON) of only 48, and a TOF of 750 µmol g^{-1} h^{-1}. Under similar reaction conditions, Re-bpy-sp^2c-COF,[30b] composed of olefin linked pyrene and bipyridine units (Figure 2h), gave a TOF of 1040 µmol g^{-1} h^{-1} (TON = 18). In these studies, the [Re(bpy)$(CO)_3$Cl]-incorporated COFs have a longer duration of catalytic activity compared to the molecular analog but only marginally higher TONs. These results suggest that Re catalyst immobilization within a COF matrix may slow or prevent unwanted dimerization deactivation pathways, but also hinders catalytic reactivity. Similar trends are observed in MOF analogs.[31] Examples of Ni, Mn, and Rh as CO_2RR active sites on bpy-linked COFs have also been reported and warrant further investigation.[32]

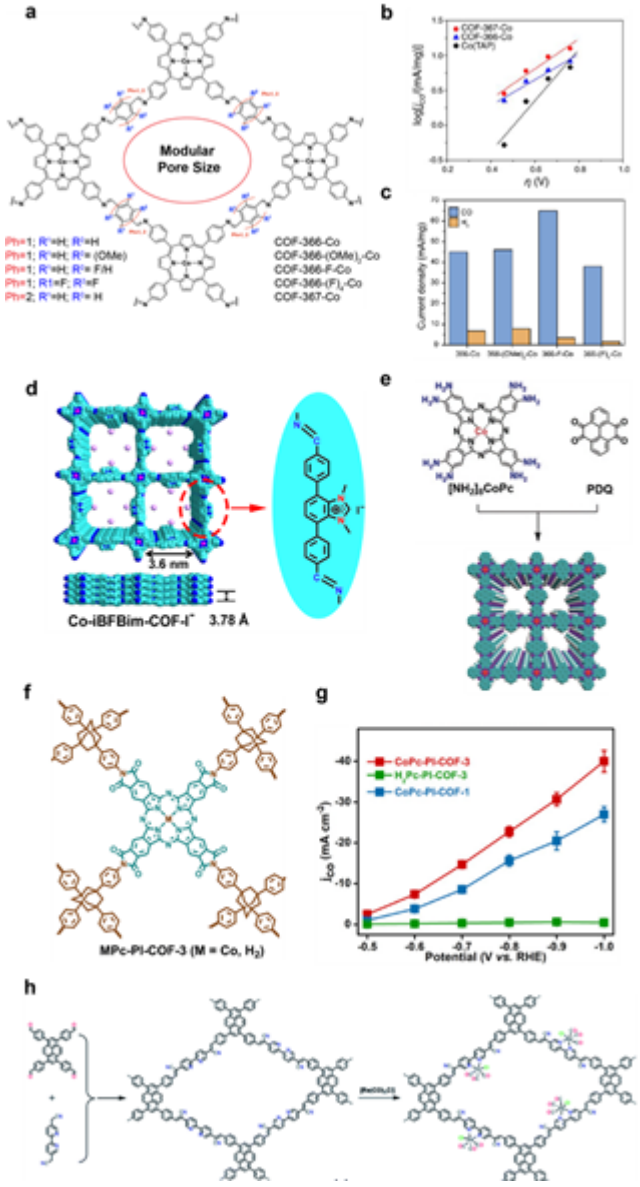

Figure 2. Representative covalent organic framework (COFs) catalysts for carbon dioxide reduction reaction (CO_2RR). (a) Chemical structures of Co complexes of COF-366, COF-367, and synthetically tuned analogs. (b) Tafel plots comparing electrochemical CO_2RR activity of COF-366-Co, COF-367-Co, and a molecular analog Co(TAP). (c) Current density comparison for COF-366-Co with reticular tuning of struts with –H, $–(OMe)_2$, –F, and $–(F)_4$ substituents. (d) Crystal structure representation of Co-iBFBim-COF-I^-. (e) Structure of

phenazine-linked phthalocyanine COF, CoPc-PDQ-COF. (f) Chemical structure of CoPc-PI-COF-3 and (f) current density plot comparing the 2D, 3D, and Co-free analogs of CoPc-PI-COF. Adapted with permission from (a, c) ref 17, © American Chemical Society 2018; (b) ref 16, © 2015 American Association for the Advancement of Science; (d) ref 25, © 2022 Wiley-VCH; (e) ref 26a, ©Wiley-VCH; (f, g) ref 26 c, © 2022 Wiley-VCH; (h) ref 30b, © 2020 Royal Society of Chemistry.

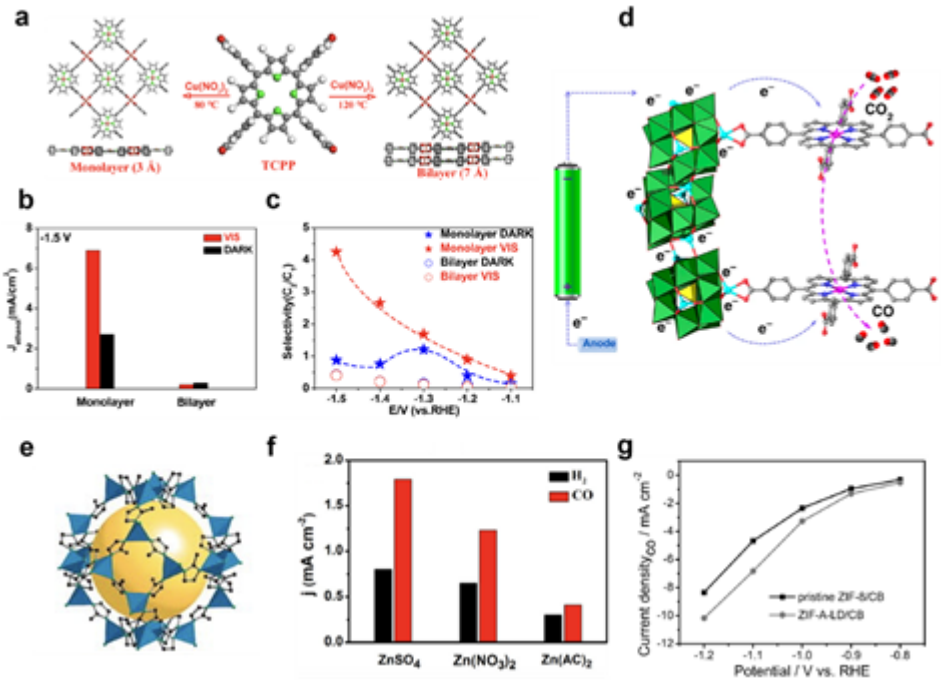

Figure 3. Representative metal organic framework catalysts for CO_2RR. (a) Monolayer and bilayer representations of Cu-porphyrin MOFs with data comparing (b) light dependent ethanol production and (c) light dependent C2/C1 selectivity ratios between the two catalyst compositions. (d) Depiction of electron transmission from an electrode through

Co-PMOF. (e) Crystal structure representation of the first reported ZIF-8 and current density plots for electrochemical CO_2RR with (f) ZIF-8 synthesized from different Zn starting material and (g) phenanthroline ligand doped (ZIF-A-LD/CB) doped versus pristine (ZIF-8/CB). Adapted with permission from (a-c) ref 34k, © 2022 Wiley-VCH; (d) ref 34e, © 2018 Springer Nature; (e) ref 36a, © 2006 National Academy of Sciences; (f) ref 36d, © 2017 Wiley-VCH (g) ref 34g, © 2019 Wiley-VCH

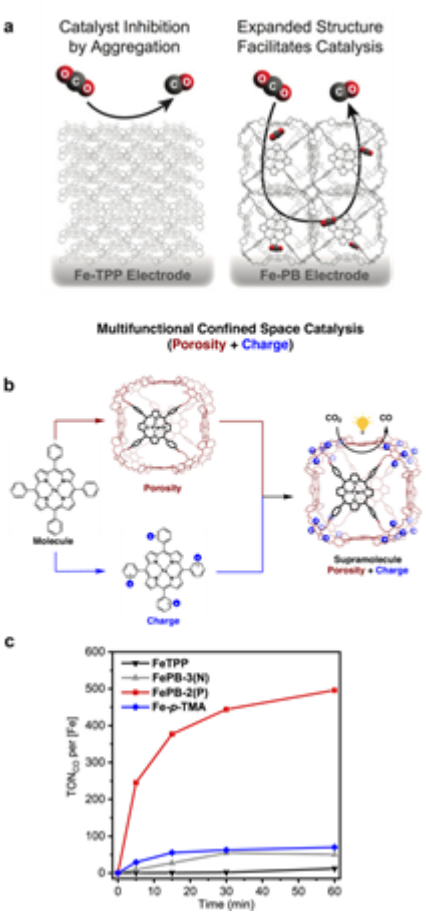

Figure 4. A representative porous molecular cage architecture to improve CO_2RR activity over monomeric molecular counterparts. (a) Proposed orientation adopted by planar Fe-TPP porphyrins compared with porous supramolecular Fe-PB on an electrode, where the 3D structure facilitates mass transport (b) Schematic representation of the planar molecular catalyst Fe-TPP transformed by porosity only (Fe-PB) or porosity and charge (Fe-PB-2(P)). (b). Photocatalytic CO_2RR results comparing activities of Fe-TPP, Fe-PB-3(N), Fe-PB-2(P), and Fe-p-TMA under a CO_2-saturated atmosphere. Adapted with permission from (a) ref 42, © 2018 Wiley-VCH; ref 43, © 2023 Wiley-VCH.

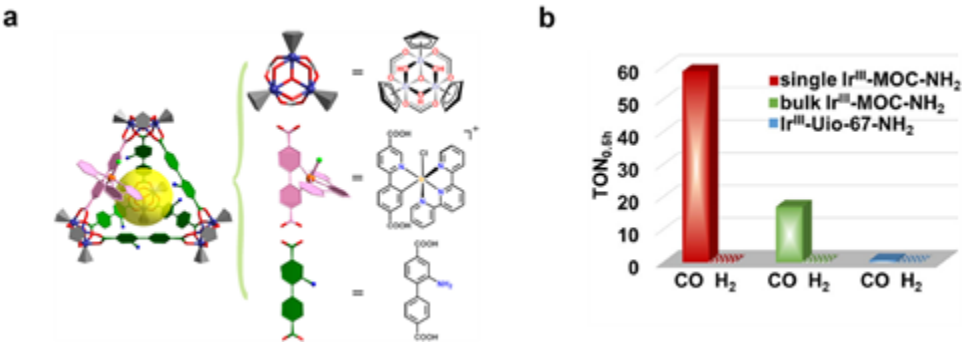

Figure 5. Representative Metal-Organic Cages for CO_2RR. (a) Structure representations of Ir^{III}-MOC-NH_2 and (b) photocatalytic CO_2RR data comparing the activity of single versus bulk Ir^{III}-MOC-NH_2, and a known MOF analog. Adapted with permission from ref 45b, © 2021 American Chemical Society.

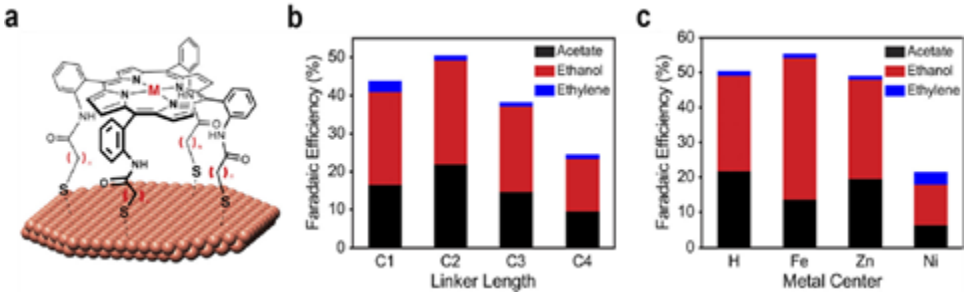

Figure 6. (a) Schematic of a hybrid molecular material exhibiting permanent porosity generated by supramolecular self-assembly between a table-shaped porphyrin molecule and an electroactive metal electrode surface. The Faradaic efficiency (FE) for value-added two-carbon products generated by C-C product formation from electrochemical CO reduction (e.g., ethylene, ethanol, acetate) is dependent on (b) molecular tuning of porphyrin linker length and (c) identity of porphyrin metal center. Reproduced with permission from ref 7i, © 2020 American Chemical Society.

Table 1. Catalytic CO_2RR Activity of Selected COF Catalysts

Catalyst	Product (Selectivity %)	TON	TOF	Energy Input*	FE (%)	QY (%)	Current Density
COF-366-Co	CO	1,352	98 h^{-1}	η= 550 mV	90	–	5 $mAmg^{-1}$
COF-366-Co oriented thin film	CO	3,542	665 h^{-1}	η= 550 mV	86	–	45 $mAmg^{-1}$
COF-367-Co	CO	3,901	165 h^{-1}	η= 550 mV	91	–	13 $mAmg^{-1}$
Co-TTCOF	CO	141,479	1.28 s^{-1}	η= 790 mV	91.3	–	1.84 $mAcm^{-2}$
Co-TTCOF NSs	CO	–	–	–0.8 V vs RHE	99.7	–	–
3D-Por(Co/H)-COF	CO	–	4610 h^{-1}	–1.1 V vs RHE	92.4	–	15.5 $mAcm^{-2}$
JUC-640-Co	CO	–	15.1 mmol $g^{-1}h^{-1}$	$Ru(bpy)_3Cl_2 \cdot 6H_2O$ at 450 nm	94.4	1.48	–
COF-300-AR	CO	–	–	–0.85 V vs RHE	83	–	2 $mAcm^{-2}$
Co-iBFBim-COF-I^-	CO (100)	–	3018 h^{-1}	2.4 V full cell voltage	99	–	52 $mAcm^{-2}$
CoPc-PDQ-COF	CO (96)	320,000	11412 h^{-1}	η= 560 mV	96	–	762 $mAmg^{-1}$
CoPc-PI-COF-3	CO	35,500	0.6 s^{-1}	–1.0 V vs RHE	96	–	31.7 $mAcm^{-2}$
Re-COF	CO (98)	48	750 μmol $g^{-1}h^{-1}$	Self-sensitized >420 nm	–	–	–
Re-bpy-sp^2c-COF	CO (81)	18.7	1040 μmol $g^{-1}h^{-1}$	Self-sensitized >420 nm	–	0.5	–

*Overpotential (η), applied potential (V vs RHE), or photosensitizer/irradiation wavelength provided

4. Metal-Organic Frameworks

Metal-organic frameworks (MOFs) are another class of extended crystalline solids that incorporate modular organic linkers, but in contrast utilize metal ions or clusters as secondary building units.[33] The similarity between these reticular materials and COFs leads to analogous MOF designs for CO_2RR applications, where the area is largely dominated by structures based on the heterogenization of porphyrin and phthalocyanine catalytic units.[15, 31a, 33g, 34]

Table 2. Catalytic CO_2RR Activity of Selected MOF Catalysts

Catalyst	Product (Selectivity %)	TON	TOF	Energy Input	FE (%)	QY (%)	Current Density
PCN-222	$HCOO^-$ (100)	–	3 μmol h^{-1}	Self-sensitized >420 nm	–	–	–
$[Al_2(OH)_2TCPP\text{-}Co]$	CO	1400	200 h^{-1}	–0.7 V vs RHE	76	–	1.8 $mAcm^{-2}$
Cu monolayer	ethanol(25.9), ethene(12)	–	–	–1.4 V vs RHE >420 nm	41.1	–	6.89 $mAcm^{-2}$ (ethanol)
Cu bilayer	CO, HCOO-	–	–	–1.3 V vs RHE >420 nm	78.6	–	0.29 $mAcm^{-2}$
Co-PMOF	CO	53,433	1656 h^{-1}	–0.8 V vs RHE	98.7	–	18.08 $mAcm^{-2}$
ZIF-8 (SO_4^{2-})	CO	–	–	–1.8 V vs SCE	65.5	–	1.55 $mAcm^{-2}$
ZIF-8 (NO_3^-)	CO	–	–	–1.8 V vs SCE	69.8	–	1.25 $mAcm^{-2}$

ZIF-8 (Acetate)	CO	–	–	–1.8 V vs SCE	57.7	–	0.5 $mAcm^{-2}$
ZIF-8 (doped)	CO	–	–	–1.1 V vs RHE	90.6	–	10 $mAcm^{-2}$

*Overpotential (η), applied potential (V vs RHE), or photosensitizer/irradiation wavelength provided

4.1. Porphyrin-based MOFs

One of the first examples of photocatalytic CO_2 reduction using a porphyrin-based MOF was reported by Jiang et al, termed PCN-222.[35] The MOF formulated as $Zr_6(\mu_3\text{-}OH)_8(OH)_8(TCPP)_2$ contains metal-free porphyrin linkers and Zr_6 cluster nodes. It was observed that incorporating TCPP into a MOF structure resulted in broad visible light absorption with higher molar absorptivity compared to H_2TCPP. Indeed, this allowed self-sensitized photochemical CO_2RR selective for formate, resulting in 30 µL of product after 10 h of irradiation. Transient absorption studies suggest that long-lived **charge transfer** states in PCN-222 prevented fast electron-hole recombination, boosting CO_2RR activity. An early example of MOFs applied to electrochemical CO_2RR was reported by Yang, Yaghi, and our laboratory. $[Al_2(OH)_2TCPP\text{-}Co]$,[34a] incorporating cobalt porphyrin molecular units linked with aluminum oxide rods in a 3D MOF structure, was fabricated into thin films of varying thickness as an integrated electrode material. MOF thickness values between 30 and 70 nm resulted in optimal conditions for CO_2-to-CO conversion with a maximum TOF of 200 h^{-1} and a stable current density over 7 h. The emphasis in examining **electrode construction** is presented as a balance between reactant diffusion and charge transport and was executed with the use of atomic layer deposition. This concept was expanded upon by the Wang laboratory using MOFs constructed from $Cu_2(COO)_4$ paddle wheels linked by Cu porphyrins (Figure 3a) .[34k] The 2D MOF was utilized as either a monolayer or a bilayer of 0.28 and 0.7 nm thickness, respectively, and demonstrated distinct product selectivity under photocoupled electrocatalysis of CO_2 reduction. Interestingly, the monolayer version favored the formation of C-C coupled products, while the bilayer generates only C-1 products (CO, CH_4, and formate). However, upon electrolysis, the authors found that within the monolayer, more active sites are accessible to the electrode, and the generation of Cu clusters is observed. Catalyst restructuring occurs at the Cu-O sites, irreversibly changing them to Cu-Cu sites that can subsequently form multi-carbon products from CO_2. Furthermore, the Faradaic efficiency

(FE) of C-C product formation from the monolayer showed light dependence (Figure 3b, c), where neither structural instability nor enhancement by irradiation is observed in the bilayer.

Returning to the discussion of **charge transfer** as a design concept for efficient CO_2RR catalysis, the use of metal clusters in MOFs is advantageous. Reductive polyoxometalates such as Z-e-Keggin cluster, ε-$PMo_8^{V}Mo_4^{VI}O_{40}Zn_4$, are electron rich aggregates that can facilitate electron transfer from the electrode to a porphyrin active site (Figure 3d). Lan and colleagues reported that the cobalt porphyrin-linked polyoxometalate MOF, Co-PMOF, shows excellent catalytic performance, with 99% FE for CO_2 to CO and a TOF of 1656 h^{-1}.[34e] The design of this CO_2RR catalyst system mirrors that of Co-TTCOF, further supporting the idea that efficient, directional **charge transfer** can be designed into molecular materials.

4.2. Zinc Imidazolate Frameworks

In related family of molecular materials, Zinc Imidazolate Frameworks (ZIFs) can enable CO_2 reduction in MOF-type materials without the need to immobilize known molecular CO_2RR catalysts.[34g, 36] ZIFs are class of MOFs based on zeolite topologies and contain Zn clusters and imidazolate ligands as building units of the framework. Specifically, the ZIF-8 congener (Figure 3e) possesses high CO_2 adsorption properties, and the tuning of peripheral components, such as electrolyte anions and ligand doping, has been studied in the context of CO_2RR. Indeed, work by Kang and colleagues on ZIF-8 generated from Zn(II) sources containing different anions (SO_4^{2-}, NO_3^-, and acetate) showed that the SO_4^{2-} derived MOF showed the highest current density for CO formation (Figure 3f), with 66% FE and catalytic stability for at least 4 hours.[36d] Additionally, varying the electrolyte anions between Cl^-, ClO_4^-, and HCO_3^- showed that use of a NaCl electrolyte achieved the highest FE for CO production, credited to more facile anion exchange within the MOF cavity. Another approach taken by Wang and co-workers towards enhancing ZIF-8 CO_2RR reactivity was ligand doping with 1,10-phenanthroline.[34g] An increase in the FE and current density (Figure 3g) for CO production from 50 to 75% was observed with phenanthroline doping, which appears to be a function of charge transfer

boosting into the imidazolate sp^2 carbons responsible for the generation of the CO_2 reduction intermediate, *COOH. We note that the studies highlighted here do not resolve the open question of whether the Zn nodes or the imidazole ligands within these catalytic ZIF cavities are the major active sites for electrochemical CO_2 reduction.

5. Porous Molecular Cages and Related Hybrid Molecular-Materials Cages

Taking extended heterogeneous molecular materials a step closer towards homogeneous molecules, porous molecular cages provide a distinct class of crystalline, microporous materials that resemble discrete analogs of MOFs and COFs. Unlike extended frameworks, porous molecular cages offer intrinsic permanent porosity in homogeneous molecular form, in which each discrete supramolecular unit can be utilized for photo- and electrocatalysis across a variety of formulations. Included are heterogeneous electrodes, particle suspensions of varying sizes, and homogeneous molecules in solution.

5.1. Porous Organic Cages

Porphyrin boxes (PB) are a prominent class of porous organic cages[37] assembled from six porphyrin face units connected by eight triamine linkers, creating a hollow box-like structure with a defined permanent inner cavity per discrete molecular unit.[38] Work from our laboratory in collaboration with Kim's group has established the use of Fe- and Co-metalated PBs for electrochemical and photochemical activation of various small molecule substrates, including oxygen,[39] nitrate,[40] and water.[41] Together we reported the first application of porous organic cages for CO_2RR activity. Specifically, the porous cage Fe-PB was formulated as a water-compatible heterogeneous electrode catalyst for direct comparison with the mononuclear analog, Fe-TPP.[7i, 42] In particular, we reasoned that creating a heterogeneous electrode material with Fe-TPP would result in stacking of flat 2D porphyrin molecules parallel to the electrode, thus limiting substrate accessibility and charge transport (Figure 4a). In contrast, owing to their permanent porosity, the porphyrin boxes would exhibit higher CO_2 substrate accessibility and **charge transport** from the electrode relative to the

porphyrin monomer. Indeed, the permanent porosity and increased surface area of the 3D porphyrin box supramolecule relative to the 2D porphyrin molecule enhanced the percentage of accessible electroactive Fe centers for the former (54% in Fe-PB, 38% in Fe-TPP). Under electrochemical CO_2RR conditions in neutral pH aqueous media, Fe-PB generated 2-fold more CO product than Fe-TPP, reaching 100% FE and achieving TOF values of 0.64 s^{-1} while maintaining electrochemical activity for at least 24 hours.

Building upon these results, we were successful in attempts to solubilize Fe-PB-like structures for homogeneous CO_2RR catalysis by the incorporation of 24 cationic trimethylammonium groups to furnish Fe-PB-2(P); we then evaluated this porous cage under photocatalytic CO_2RR conditions (Figure 4b).[43] The highly cationic, soluble porphyrin box platform, featuring dual second-sphere additions of porosity and charge as **activating groups**, led to synergistic improvements in selective and efficient CO_2-to-CO conversion in homogeneous solution. Fe-PB-2(P) exhibited a maximum TON of 1,168 for CO production with 97% selectivity within a one-hour photolysis experiment using $Ir(ppy)_3$ as a photosensitizer. The direct comparison of Fe-PB-2(P), featuring both porosity and charge, to the porosity-only porphyrin box Fe-PB-3(N), the charged-only mononuclear porphyrin Fe-*p*-TMA, and the parent Fe-TPP analog showed that Fe-PB-2(P) exhibited a 41-fold higher activity over Fe-TPP (Figure 4c) with a maximum TON of ca. 500, with the neutral porous FePB-3(N) and charged mononuclear Fe-*p*-TMA catalysts displaying similar levels of activity under these conditions, with 4-fold (TON = 50) and 6-fold (TON= 70) higher CO_2RR activities compared to Fe-TPP, respectively. Taken together, these results established that integrating dual porosity and electrostatic interactions as **activating groups** onto a single platform can work in tandem to enhance photocatalytic CO_2RR activity in synergistic manner beyond introduction of a single porosity or electrostatic design element alone. Finally, the Fe-PB-2(P) catalyst also enabled photochemical CO_2RR activity under low CO_2 concentrations. Indeed, in the presence of as little as 2% CO_2 in acetonitrile solution, Fe-PB-2(P) retained up to 78% of its original activity compared to CO_2-saturated conditions, suggesting that the porous organic cage platforms can promote both carbon capture and conversion.

Table 3. Catalytic CO_2RR Activity of Selected Porous Molecular Cages and Hybrid Materials

Catalyst	Product (Selectivity %)	TON	TOF	Energy Input*	FE (%)	QY (%)	Current Density
Fe-PB	CO	55,250	0.64 s^{-1}	η =510 mV	100		0.4 $mAcm^{-2}$
Fe-PB-2P	CO (97)	1,168	164 min^{-1}	$Ir(ppy)_3$ at 450 nm	–	5.75	–
Fe-PB-3N	CO (88)	50	1.9 min^{-1}	$Ir(ppy)_3$ at 450 nm	–	–	–
ReTC-MOP	CO	12,847	660 h^{-1}	Self-sensitized >420 nm	–	–	–
ReTC MOF_{nano}	CO	654	36 h^{-1}	Self-sensitized >420 nm	–	–	–
ReTC MOF_{micro}	CO	438	24 h^{-1}	Self-sensitized >420 nm	–	–	–
Ir^{III}-MOC-NH_2 single	CO (99)	59	120 h^{-1}	Self-sensitized 420 nm		6.71	
Ir^{III}-MOC-$NH_{2\ bulk}$	CO (96)	20	–	Self-sensitized 420 nm	–	–	–
Fe Cap, C2 linker	Ethanol (53)**	–	–	–0.40 V vs RHE	83	–	1.34 $mAcm^{-2}$
	Acetate (24)**						

*Overpotential (η), applied potential (V vs RHE), or photosensitizer/irradiation wavelength provided

** refers to the Faradaic efficiency (FE) values

5.2. Metal-Organic Cages/Metal-Organic Polyhedra

Metal-organic cages (MOC), otherwise known as metal-organic polyhedra (MOP), are reticular structures featuring connections between organic linkers and inorganic joints, and can be thought of as discrete molecular analogs of MOFs.[33g, 44] Like porous organic cages, MOCs/MOPs feature intrinsic permanent porosity and can be used to make heterogeneous analogs of molecular catalysts.[45] For example, efficient CO_2RR catalysis from heterogenized Re-bpy catalysts can be achieved under photocatalytic conditions. Choi and colleagues designed a MOP structure using the Zr cluster ($[Cp_3Zr_3O(OH)_3(CO_2)_3]^+$) linked with biphenyldicarboxylate (BPDC) struts; one BPDC unit was substituted with a carboxylate functionalized version of $[Re(CO)_3(bpy)(Cl)]$, forming 1.8 nm particles of ReTC-MOP.[45a] The self-sensitized photocatalyst ReTC-MOP with molecular-like **light absorption** properties displayed a TON of 12,847 for CO production over a 24-hour photolysis experiment in acetonitrile solution. The observed high activity far surpassed the molecular analog, as well as nano (400 nm) and micro-scaled (400 μm) ReTC MOF particles constructed for comparison to ReTC-MOP. The authors speculated that the reaction microenvironment of MOP particles dispersed in solution could permit better access of CO_2 to the active site. Further dilution of MOP/MOC particles to single cages by Su and colleagues was shown to increase utilization efficiency in Ir^{III}-MOC-NH_2.[45b] The MOC in this case comprises four $Cp_3Zr_3\mu_3$-$O(\mu_2$-$OH)_3$ nodes linked by an Ir(III) polypyridyl complex and amino-functionalized BPDC (Figure 5a). Photocatalytic assays showed a 3.4-fold improvement in TOF for a single-cage MOC unit versus bulk Ir^{III}-MOC-NH_2 (Figure 5b). DFT analysis of possible mechanistic pathways suggested that the free amines in the cage can enhance CO_2 reduction by acting as **activating groups** for increased CO_2 capture, akin to what was proposed for COF-300-AR.[23]

5.3. Molecular-Materials Cages

A final series of porous molecular materials to highlight for CO_2 reduction chemistry are hybrid combinations of discrete molecules or cages with materials surfaces. Such systems are comprised of molecules that can directly interact with a CO_2RR-active electrode to provide systems that exhibit permanent porosity and electrochemical activity, improving both **mass transport** and **charge transfer**.[7i, 37d, 46] In one study, our laboratory developed hybrid molecular-materials porphyrin

molecular cages that were formed between α,α,α,α-atropisomers of thioacetate-functionalized porphyrins and a metal foil electrode. The thiols on the legs of the table-shaped porphyrin molecule bind the electrode surface, fixing the porphyrins parallel to the electrode surface at synthetically modular distances (Figure 6a).[46a] Using copper foil electrodes, we evaluated the reduction of CO to value-added two-carbon products formed from C-C coupling (e.g., ethylene, ethanol, acetate) using these hybrid materials. Both bare copper and porphyrin-functionalized hybrids produced ethylene, ethanol, and acetate upon electrochemical CO reduction, but the addition of porosity created by the supramolecular porphyrin cage structures led to a marked increase in FE for the latter two C-C oxygenated products. Molecular optimization of linker length (1-4 carbon chains) showed that the C2 linker produced optimal Faradaic efficiencies to maximize two-carbon product formation (Figure 6b). We then used the C2-spaced porphyrin cap to probe multimetallic catalysis by inserting Fe, Ni, or Zn into the center of the porphyrin cap. Insertion of Fe as a secondary **activating group** resulted in an increased ethanol selectivity, reaching 52% FE (Figure 6c). Various control experiments using porphyrin isomers without the proper electrode capping configuration, or porphyrins without the coordinating thiol caps, were evaluated to corroborate the importance of porous cage formation for the observed results. In related work by Reisner, Scherman, and Han, among others, porous organic cages and cucurbit[n]urils have been used as additives to enhance CO_2 diffusion at the surfaces of Cu and Au electrodes, respectively. Interestingly, only the CC3[37d] porous organic cage resulted in more efficient CO_2RR catalysis, whereas cucurbit[6]uril[46b] caused a decrease in current density.

6. Summary and Perspectives

Molecular materials are emerging as valuable class of CO_2 reduction catalysts that can be driven by sustainable electrical or solar input. Indeed, these systems merge two of the most important aspects in the development of functional catalysts: modularity and durability. In particular, the development of functional molecular materials catalysts that exhibit permanent porosity, including COFs, MOFs, and porous molecular cages, have led to advances in design principles that exploit both the molecular precision afforded in homogeneous systems and the durability of heterogenous

counterparts. In the context of CO_2RR, a key property in the molecular materials space is porosity, which can enhance the diffusion and/or capture of CO_2 substrate and funnel it towards the active site of the catalyst. Furthermore, examples highlighted in this mini-review leverage the molecular modularity of these porous materials systems via implementation of directional charge transfer, second-sphere cationic interactions, CO_2 capture and activating groups, pore size manipulation, and dimensionality.

Moving forward, many exciting opportunities merit further investigation to achieve significant advances in molecular materials for CO_2RR chemistry and related small-molecule transformations of energy consequence. First and foremost is the development of systems that can go beyond two-electron reduction, as the vast majority of molecular materials for catalytic CO_2RR are limited to producing CO, akin to their pure molecular counterparts. Indeed, the immobilization of a relatively small subset of well-established molecular catalysts as active sites in these materials has been studied extensively, therefore future efforts in the field should seek to heterogenize the rapidly emerging body of new state-of-the-art molecular catalysts into porous structures. Another common challenge arising in these molecularly-designed materials is how to optimize the construction of electrodes in order to increase conductivity of the material and electroactivity of catalytic sites. Additionally, as has been repeatedly observed in porous molecular cages, devoting more attention to contributions of the secondary coordination sphere and leveraging these confined space microenvironments is an important new development in enhancing CO_2RR reactivity. In this context, inspiration from recently generated molecular coordination complexes that append hydrogen bonding and/or electrostatic moieties that aid CO_2 reduction offers a molecular-to-materials roadmap for developing next-generation catalysts for combined carbon capture and fixation. These and other avenues of basic and translation energy research will bring us closer to the larger goal of decarbonizing our global energy infrastructure, of which CO_2RR catalysis is but one part of the puzzle.

Acknowledgements

This work was supported by the U.S. Department of Energy, Office of Science, Office of Advanced Scientific Computing, Office of Basic Energy Sciences, via the Division of Chemical Sciences, Geosciences, and Bioscience of the U.S. Department of Energy at Lawrence Berkeley National Laboratory (Grant No. DE-AC02-05CH11231 to C.J.C.). P.D. acknowledges the NSF for a Graduate Research Fellowship. C.J.C. is a CIFAR Fellow.

References:

[1] (a) S. Chu, Y. Cui, N. Liu, *Nat. Mater.* **2017**, *16*, 16-22 (b) P. Janoska, IEA, **2019** (c) N. Zhao, F. You, *Appl. Energy* **2020**, *279*, 115889 (d) M. J. B. Kabeyi, O. A. Olanrewaju, *Front. Energy Res.* **2022**, *9* (e) L. De La Peña, R. Guo, X. Cao, X. Ni, W. Zhang, *Resour. Conserv. Recycl.* **2022**, *177*, 105957.

[2] (a) A. Majumdar, J. Deutch, *Joule* **2018**, *2*, 805-809 (b) P. De Luna, C. Hahn, D. Higgins, A. Jaffer Shaffiq, F. Jaramillo Thomas, H. Sargent Edward, *Science* **2019**, *364*, eaav3506.

[3] (a) N. Mac Dowell, P. S. Fennell, N. Shah, G. C. Maitland, *Nat. Clim. Change* **2017**, *7*, 243-249 (b) P. Gabrielli, M. Gazzani, M. Mazzotti, *Ind. Eng. Chem. Res.* **2020**, *59*, 7033-7045.

[4] (a) E. E. Benson, C. P. Kubiak, A. J. Sathrum, J. M. Smieja, *Chem. Soc. Rev.* **2009**, *38*, 89-99 (b) A. M. Appel, J. E. Bercaw, A. B. Bocarsly, H. Dobbek, D. L. DuBois, M. Dupuis, J. G. Ferry, E. Fujita, R. Hille, P. J. A. Kenis, C. A. Kerfeld, R. H. Morris, C. H. F. Peden, A. R. Portis, S. W. Ragsdale, T. B. Rauchfuss, J. N. H. Reek, L. C. Seefeldt, R. K. Thauer, G. L. Waldrop, *Chem. Rev.* **2013**, *113*, 6621-6658 (c) C. Costentin, M. Robert, J.-M. Savéant, *Chem. Soc. Rev.* **2013**, *42*, 2423-2436 (d) S. Nitopi, E. Bertheussen, S. B. Scott, X. Liu, A. K. Engstfeld, S. Horch, B. Seger, I. E. L. Stephens, K. Chan, C. Hahn, J. K. Nørskov, T. F. Jaramillo, I. Chorkendorff, *Chem. Rev.* **2019**, *119*, 7610-7672 (e) A. H. Proppe, Y. C. Li, A. Aspuru-Guzik, C. P. Berlinguette, C. J. Chang, R. Cogdell, A. G. Doyle, J. Flick, N. M. Gabor, R. van Grondelle, S. Hammes-Schiffer, S. A. Jaffer, S. O. Kelley, M. Leclerc, K. Leo, T. E. Mallouk, P. Narang, G. S. Schlau-Cohen, G. D. Scholes, A. Vojvodic, V. W.-W. Yam, J. Y. Yang, E. H. Sargent, *Nat. Rev. Mat.* **2020**, *5*, 828-846 (f) H. S. Shafaat, J. Y. Yang, *Nat. Catal.* **2021**, *4*, 928-933 (g) E. W. Lees, B. A. W. Mowbray, F. G. L. Parlane, C. P. Berlinguette, *Nat. Rev. Mat.* **2022**, *7*, 55-64.

[5] P. Saha, S. Amanullah, A. Dey, *Acc. Chem. Res.* **2022**, *55*, 134-144.

[6] H. Takeda, C. Cometto, O. Ishitani, M. Robert, *ACS Catal.* **2017**, *7*, 70-88.

[7] (a) A. Taheri, L. A. Berben, *Inorg. Chem.* **2016**, *55*, 378-385 (b) I. Azcarate, C. Costentin, M. Robert, J.-M. Savéant, *J. Am. Chem. Soc.* **2016**, *138*, 16639-16644 (c) R. Francke, B. Schille, M. Roemelt, *Chem. Rev.* **2018**, *118*, 4631-4701 (d) A. W. Nichols, C. W. Machan, *Front. Chem.* **2019**, *7* (e) J. M. Barlow, J. Y. Yang, *ACS Cent. Sci* **2019**, *5*, 580-588 (f) C. G. Margarit, C. Schnedermann, N. G. Asimow, D. G. Nocera, *Organometallics* **2019**, *38*, 1219-1223 (g) E. Boutin, L. Merakeb, B. Ma, B. Boudy, M. Wang, J. Bonin, E. Anxolabéhère-Mallart, M. Robert, *Chem. Soc. Rev.* **2020**, *49*, 5772-5809 (h) P. Gotico, Z. Halime, A. Aukauloo, *J. Chem. Soc., Dalton Trans.* **2020**, *49*, 2381-2396 (i) P. T. Smith, E. M. Nichols, Z. Cao, C. J. Chang, *Acc. Chem. Res.* **2020**, *53*, 575-587.

[8] (a) Y. Hori, in *Modern Aspects of Electrochemistry* (Eds.: C. G. Vayenas, R. E. White, M. E. Gamboa-Aldeco), Springer New York, New York, NY, **2008**, pp. 89-189 (b) D. D. Zhu, J. L. Liu, S. Z. Qiao, *Adv. Mater.* **2016**, *28*, 3423-3452 (c) L. Zhang, Z.-J. Zhao, J. Gong, *Angew. Chem. Int. Ed.* **2017**, *56*, 11326-11353 (d) K. Jiang, R. B. Sandberg, A. J. Akey, X. Liu, D. C. Bell, J. K. Nørskov, K. Chan, H. Wang, *Nat. Catal.* **2018**, *1*, 111-119 (e) S. Zhao, R. Jin, R. Jin, *ACS Energy Lett.* **2018**, *3*, 452-462 (f) M. Li, H. Wang, W. Luo, P. C. Sherrell, J. Chen, J. Yang, *Adv. Mater.* **2020**, *32*, 2001848 (g) J. E. Huang, F. Li, A. Ozden, A. Sedighian Rasouli, F. P. García de Arquer, S. Liu, S. Zhang, M. Luo, X. Wang, Y. Lum, Y. Xu, K. Bertens, R. K. Miao, C.-T. Dinh, D. Sinton, E. H. Sargent, *Science* **2021**, *372*, 1074-1078.

[9] (a) C. S. Diercks, Y. Liu, K. E. Cordova, O. M. Yaghi, *Nat. Mater.* **2018**, *17*, 301-307 (b) A. Wagner, C. D. Sahm, E. Reisner, *Nat. Catal.* **2020**, *3*, 775-786 (c) S. Zhang, Q. Fan, R. Xia, T. J. Meyer, *Acc. Chem. Res.* **2020**, *53*, 255-264 (d) D.-H. Nam, P. De Luna, A. Rosas-Hernández, A. Thevenon, F. Li, T. Agapie, J. C. Peters, O. Shekhah, M. Eddaoudi, E. H. Sargent, *Nat. Mater.* **2020**, *19*, 266-276.

[10] (a) D. Gao, R. M. Arán-Ais, H. S. Jeon, B. Roldan Cuenya, *Nat. Catal.* **2019**, *2*, 198-210 (b) X. Zhang, S.-X. Guo, K. A. Gandionco, A. M. Bond, J. Zhang, *Materials Today Advances* **2020**, *7*, 100074 (c) L. Fan, C. Xia, F. Yang, J. Wang, H. Wang, Y. Lu, *Science Advances* **2020**, *6*, eaay3111 (d) Y. Xue, Y. Guo, H. Cui, Z. Zhou, *Small Methods* **2021**, *5*, 2100736 (e) H. Xiong, Y. Dong, D. Liu, R. Long, T. Kong, Y. Xiong, *J. Phys. Chem. Lett.* **2022**, *13*, 1272-1282 (f) J. Wang, Y. Shi, Y. Wang, Z. Li, *ACS Energy Lett.* **2022**, *7*, 2043-2059 (g) D. Bagchi, S. Roy, S. C. Sarma, S. C. Peter, *Adv. Funct. Mater.* **2022**, *32*, 2209023 (h) S. Banerjee, C. S. Gerke, V. S. Thoi, *Acc. Chem. Res.* **2022**, *55*, 504-515.

[11] (a) C. S. Diercks, O. M. Yaghi, *Science* **2017**, *355*, eaal1585 (b) O. M. Yaghi, *ACS Cent. Sci* **2019**, *5*, 1295-1300 (c) C. Gropp, S. Canossa, S. Wuttke, F. Gándara, Q. Li, L. Gagliardi, O. M. Yaghi, *ACS Cent. Sci* **2020**, *6*, 1255-1273 (d) R. Freund, S. Canossa, S. M. Cohen, W. Yan, H. Deng, V. Guillerm, M. Eddaoudi, D. G. Madden, D. Fairen-Jimenez, H. Lyu, L. K. Macreadie, Z. Ji, Y.

Zhang, B. Wang, F. Haase, C. Wöll, O. Zaremba, J. Andreo, S. Wuttke, C. S. Diercks, *Angew. Chem. Int. Ed.* **2021**, *60*, 23946-23974.

[12] A. P. Côté, A. I. Benin, N. W. Ockwig, M. O'Keeffe, A. J. Matzger, O. M. Yaghi, *Science* **2005**, *310*, 1166-1170.

[13] (a) J. W. Colson, A. R. Woll, A. Mukherjee, M. P. Levendorf, E. L. Spitler, V. B. Shields, M. G. Spencer, J. Park, W. R. Dichtel, *Science* **2011**, *332*, 228-231 (b) C. R. DeBlase, K. E. Silberstein, T.-T. Truong, H. D. Abruña, W. R. Dichtel, *J. Am. Chem. Soc.* **2013**, *135*, 16821-16824 (c) S. Dalapati, E. Jin, M. Addicoat, T. Heine, D. Jiang, *J. Am. Chem. Soc.* **2016**, *138*, 5797-5800 (d) X. Guan, F. Chen, Q. Fang, S. Qiu, *Chem. Soc. Rev.* **2020**, *49*, 1357-1384 (e) K. Geng, T. He, R. Liu, S. Dalapati, K. T. Tan, Z. Li, S. Tao, Y. Gong, Q. Jiang, D. Jiang, *Chem. Rev.* **2020**, *120*, 8814-8933 (f) M. Lu, M. Zhang, J. Liu, Y. Chen, J.-P. Liao, M.-Y. Yang, Y.-P. Cai, S.-L. Li, Y.-Q. Lan, *Angew. Chem. Int. Ed.* **2022**, *61*, e202200003 (g) Y.-R. Wang, H.-M. Ding, S.-N. Sun, J.-w. Shi, Y.-L. Yang, Q. Li, Y. Chen, S.-L. Li, Y.-Q. Lan, *Angew. Chem. Int. Ed.* **2022**, *61*, e202212162.

[14] (a) D. Behar, T. Dhanasekaran, P. Neta, C. M. Hosten, D. Ejeh, P. Hambright, E. Fujita, *J. Phys. Chem. A* **1998**, *102*, 2870-2877 (b) C. Costentin, S. Drouet, M. Robert, J.-M. Savéant, *Science* **2012**, *338*, 90-94 (c) C. Costentin, G. Passard, M. Robert, J.-M. Savéant, *Proc. Natl. Acad. Sci.* **2014**, *111*, 14990-14994 (d) G. F. Manbeck, E. Fujita, *J. Porphyr. Phthalocyanines* **2015**, *19*, 45-64 (e) C. Costentin, M. Robert, J.-M. Savéant, A. Tatin, *Proc. Natl. Acad. Sci.* **2015**, *112*, 6882-6886 (f) N. Morlanés, K. Takanabe, V. Rodionov, *ACS Catal.* **2016**, *6*, 3092-3095 (g) H. Rao, L. C. Schmidt, J. Bonin, M. Robert, *Nature* **2017**, *548*, 74-77 (h) X. Zhang, Z. Wu, X. Zhang, L. Li, Y. Li, H. Xu, X. Li, X. Yu, Z. Zhang, Y. Liang, H. Wang, *Nat. Commun.* **2017**, *8*, 14675 (i) E. M. Nichols, J. S. Derrick, S. K. Nistanaki, P. T. Smith, C. J. Chang, *Chem. Sci* **2018**, *9*, 2952-2960 (j) M. Wang, K. Torbensen, D. Salvatore, S. Ren, D. Joulié, F. Dumoulin, D. Mendoza, B. Lassalle-Kaiser, U. Işci, C. P. Berlinguette, M. Robert, *Nat. Commun.* **2019**, *10*, 3602 (k) P. Gotico, B. Boitrel, R. Guillot, M. Sircoglou, A. Quaranta, Z. Halime, W. Leibl, A. Aukauloo, *Angew. Chem. Int. Ed.* **2019**, *58*, 4504-4509 (l) P. Gotico, L. Roupnel, R. Guillot, M. Sircoglou, W. Leibl, Z. Halime, A. Aukauloo, *Angew. Chem. Int. Ed.* **2020**, *59*, 22451-22455 (m) S. Amanullah, P. Saha, A. Dey, *J. Am. Chem. Soc.* **2021**, *143*, 13579-13592 (n) J. S. Derrick, M. Loipersberger, S. K. Nistanaki, A. V. Rothweiler, M. Head-Gordon, E. M. Nichols, C. J. Chang, *J. Am. Chem. Soc.* **2022**, *144*, 11656-11663 (o) M. R. Narouz, P. De La Torre, L. An, C. J. Chang, *Angew. Chem. Int. Ed.* **2022**, *61*, e202207666.

[15] Z. Liang, H.-Y. Wang, H. Zheng, W. Zhang, R. Cao, *Chem. Soc. Rev.* **2021**, *50*, 2540-2581.

[16] S. Lin, C. S. Diercks, Y.-B. Zhang, N. Kornienko, E. M. Nichols, Y. Zhao, A. R. Paris, D. Kim, P. Yang, O. M. Yaghi, C. J. Chang, *Science* **2015**, *349*, 1208-1213.

[17] C. S. Diercks, S. Lin, N. Kornienko, E. A. Kapustin, E. M. Nichols, C. Zhu, Y. Zhao, C. J. Chang, O. M. Yaghi, *J. Am. Chem. Soc.* **2018**, *140*, 1116-1122.

[18] H.-J. Zhu, M. Lu, Y.-R. Wang, S.-J. Yao, M. Zhang, Y.-H. Kan, J. Liu, Y. Chen, S.-L. Li, Y.-Q. Lan, *Nat. Commun.* **2020**, *11*, 497.

[19] Y.-R. Wang, H.-M. Ding, X.-Y. Ma, M. Liu, Y.-L. Yang, Y. Chen, S.-L. Li, Y.-Q. Lan, *Angew. Chem. Int. Ed.* **2022**, *61*, e202114648.

[20] (a) G. Lin, H. Ding, R. Chen, Z. Peng, B. Wang, C. Wang, *J. Am. Chem. Soc.* **2017**, *139*, 8705-8709 (b) S.-Y. Chi, Q. Chen, S.-S. Zhao, D.-H. Si, Q.-J. Wu, Y.-B. Huang, R. Cao, *J. Mater. Chem. A* **2022**, *10*, 4653-4659.

[21] J. Ding, X. Guan, J. Lv, X. Chen, Y. Zhang, H. Li, D. Zhang, S. Qiu, H.-L. Jiang, Q. Fang, *J. Am. Chem. Soc.* **2023**, *145*, 3248-3254.

[22] (a) D. M. D'Alessandro, B. Smit, J. R. Long, *Angew. Chem. Int. Ed.* **2010**, *49*, 6058-6082 (b) T. M. McDonald, W. R. Lee, J. A. Mason, B. M. Wiers, C. S. Hong, J. R. Long, *J. Am. Chem. Soc.* **2012**, *134*, 7056-7065 (c) S. D. Kenarsari, D. Yang, G. Jiang, S. Zhang, J. Wang, A. G. Russell, Q. Wei, M. Fan, *RSC Advances* **2013**, *3*, 22739-22773 (d) B. Dutcher, M. Fan, A. G. Russell, *ACS Appl. Mater. Interfaces* **2015**, *7*, 2137-2148 (e) T. M. McDonald, J. A. Mason, X. Kong, E. D. Bloch, D. Gygi, A. Dani, V. Crocellà, F. Giordanino, S. O. Odoh, W. S. Drisdell, B. Vlaisavljevich, A. L. Dzubak, R. Poloni, S. K. Schnell, N. Planas, K. Lee, T. Pascal, L. F. Wan, D. Prendergast, J. B. Neaton, B. Smit, J. B. Kortright, L. Gagliardi, S. Bordiga, J. A. Reimer, J. R. Long, *Nature* **2015**, *519*, 303-308 (f) E. S. Sanz-Pérez, C. R. Murdock, S. A. Didas, C. W. Jones, *Chem. Rev.* **2016**, *116*, 11840-11876.

[23] H. Liu, J. Chu, Z. Yin, X. Cai, L. Zhuang, H. Deng, *Chem* **2018**, *4*, 1696-1709.

[24] Y.-N. Gong, W. Zhong, Y. Li, Y. Qiu, L. Zheng, J. Jiang, H.-L. Jiang, *J. Am. Chem. Soc.* **2020**, *142*, 16723-16731.

[25] Q.-J. Wu, D.-H. Si, Q. Wu, Y.-L. Dong, R. Cao, Y.-B. Huang, *Angew. Chem. Int. Ed.* **2023**, *62*, e202215687.

[26] (a) N. Huang, K. H. Lee, Y. Yue, X. Xu, S. Irle, Q. Jiang, D. Jiang, *Angew. Chem. Int. Ed.* **2020**, *59*, 16587-16593 (b) B. Han, X. Ding, B. Yu, H. Wu, W. Zhou, W. Liu, C. Wei, B. Chen, D. Qi, H. Wang, K. Wang, Y. Chen, B. Chen, J. Jiang, *J. Am. Chem. Soc.* **2021**, *143*, 7104-7113 (c) B. Han, Y. Jin, B. Chen, W. Zhou, B. Yu, C. Wei, H. Wang, K. Wang, Y. Chen, B. Chen, J. Jiang, *Angew. Chem. Int. Ed.* **2022**, *61*, e202114244.

[27] (a) J. Hawecker, J.-M. Lehn, R. Ziessel, *J. Chem. Soc., Chem. Commun.* **1984**, 328-330 (b) J. A. Barrett, C. J. Miller, C. P. Kubiak, *Trends in Chemistry* **2021**, *3*, 176-187.

[28] (a) E. E. Benson, C. P. Kubiak, *Chem. Commun.* **2012**, *48*, 7374-7376 (b) M. D. Sampson, A. D. Nguyen, K. A. Grice, C. E. Moore, A. L. Rheingold, C. P. Kubiak, *J. Am. Chem. Soc.* **2014**, *136*, 5460-5471 (c) J. D. Shipp, H. Carson, S. J. P. Spall, S. C. Parker, D. Chekulaev, N. Jones, M. Y. Mel'nikov, C. C. Robertson, A. J. H. M. Meijer, J. A. Weinstein, *J. Chem. Soc., Dalton Trans.* **2020**, *49*, 4230-4243.

[29] D. A. Popov, J. M. Luna, N. M. Orchanian, R. Haiges, C. A. Downes, S. C. Marinescu, *J. Chem. Soc., Dalton Trans.* **2018**, *47*, 17450-17460.

[30] (a) S. Yang, W. Hu, X. Zhang, P. He, B. Pattengale, C. Liu, M. Cendejas, I. Hermans, X. Zhang, J. Zhang, J. Huang, *J. Am. Chem. Soc.* **2018**, *140*, 14614-14618 (b) Z. Fu, X. Wang, A. M. Gardner, X. Wang, S. Y. Chong, G. Neri, A. J. Cowan, L. Liu, X. Li, A. Vogel, R. Clowes, M. Bilton, L. Chen, R. S. Sprick, A. I. Cooper, *Chem. Sci* **2020**, *11*, 543-550.

[31] (a) K. M. Choi, D. Kim, B. Rungtaweevoranit, C. A. Trickett, J. T. D. Barmanbek, A. S. Alshammari, P. Yang, O. M. Yaghi, *J. Am. Chem. Soc.* **2017**, *139*, 356-362 (b) P. M. Stanley, C. Thomas, E. Thyrhaug, A. Urstoeger, M. Schuster, J. Hauer, B. Rieger, J. Warnan, R. A. Fischer, *ACS Catal.* **2021**, *11*, 871-882.

[32] (a) W. Zhong, R. Sa, L. Li, Y. He, L. Li, J. Bi, Z. Zhuang, Y. Yu, Z. Zou, *J. Am. Chem. Soc.* **2019**, *141*, 7615-7621 (b) G. C. Dubed Bandomo, S. S. Mondal, F. Franco, A. Bucci, V. Martin-Diaconescu, M. A. Ortuño, P. H. van Langevelde, A. Shafir, N. López, J. Lloret-Fillol, *ACS Catal.* **2021**, *11*, 7210-7222 (c) Z. Zhao, D. Zheng, M. Guo, J. Yu, S. Zhang, Z. Zhang, Y. Chen, *Angew. Chem. Int. Ed.* **2022**, *61*, e202200261.

[33] (a) B. F. Hoskins, R. Robson, *J. Am. Chem. Soc.* **1990**, *112*, 1546-1554 (b) H. Li, M. Eddaoudi, M. O'Keeffe, O. M. Yaghi, *Nature* **1999**, *402*, 276-279 (c) O. M. Yaghi, H. Li, *J. Am. Chem. Soc.* **1995**, *117*, 10401-10402 (d) P. Horcajada, T. Chalati, C. Serre, B. Gillet, C. Sebrie, T. Baati, J. F. Eubank, D. Heurtaux, P. Clayette, C. Kreuz, J.-S. Chang, Y. K. Hwang, V. Marsaud, P.-N. Bories, L. Cynober, S. Gil, G. Férey, P. Couvreur, R. Gref, *Nat. Mater.* **2010**, *9*, 172-178 (e) H. Furukawa, N. Ko, Y. B. Go, N. Aratani, S. B. Choi, E. Choi, A. Ö. Yazaydin, R. Q. Snurr, M. O'Keeffe, J. Kim, O. M. Yaghi, *Science* **2010**, *329*, 424-428 (f) H.-C. Zhou, J. R. Long, O. M. Yaghi, *Chem. Rev.* **2012**, *112*, 673-674 (g) T. R. Cook, Y.-R. Zheng, P. J. Stang, *Chem. Rev.* **2013**, *113*, 734-777 (h) H.-C. J. Zhou, S. Kitagawa, *Chem. Soc. Rev.* **2014**, *43*, 5415-5418 (i) A. E. Baumann, D. A. Burns, B. Liu, V. S. Thoi, *Commun. Chem* **2019**, *2*, 86.

[34] (a) N. Kornienko, Y. Zhao, C. S. Kley, C. Zhu, D. Kim, S. Lin, C. J. Chang, O. M. Yaghi, P. Yang, *J. Am. Chem. Soc.* **2015**, *137*, 14129-14135 (b) C. A. Trickett, A. Helal, B. A. Al-Maythalony, Z. H.

Yamani, K. E. Cordova, O. M. Yaghi, *Nat. Rev. Mat.* **2017**, *2*, 17045 (c) M. B. Majewski, A. W. Peters, M. R. Wasielewski, J. T. Hupp, O. K. Farha, *ACS Energy Lett.* **2018**, *3*, 598-611 (d) B.-X. Dong, S.-L. Qian, F.-Y. Bu, Y.-C. Wu, L.-G. Feng, Y.-L. Teng, W.-L. Liu, Z.-W. Li, *ACS Applied Energy Materials* **2018**, *1*, 4662-4669 (e) Y.-R. Wang, Q. Huang, C.-T. He, Y. Chen, J. Liu, F.-C. Shen, Y.-Q. Lan, *Nat. Commun.* **2018**, *9*, 4466 (f) R. Matheu, E. Gutierrez-Puebla, M. Á. Monge, C. S. Diercks, J. Kang, M. S. Prévot, X. Pei, N. Hanikel, B. Zhang, P. Yang, O. M. Yaghi, *J. Am. Chem. Soc.* **2019**, *141*, 17081-17085 (g) S. Dou, J. Song, S. Xi, Y. Du, J. Wang, Z.-F. Huang, Z. J. Xu, X. Wang, *Angew. Chem. Int. Ed.* **2019**, *58*, 4041-4045 (h) H. Zhong, M. Ghorbani-Asl, K. H. Ly, J. Zhang, J. Ge, M. Wang, Z. Liao, D. Makarov, E. Zschech, E. Brunner, I. M. Weidinger, J. Zhang, A. V. Krasheninnikov, S. Kaskel, R. Dong, X. Feng, *Nat. Commun.* **2020**, *11*, 1409 (i) J. Li, H. Huang, W. Xue, K. Sun, X. Song, C. Wu, L. Nie, Y. Li, C. Liu, Y. Pan, H.-L. Jiang, D. Mei, C. Zhong, *Nat. Catal.* **2021**, *4*, 719-729 (j) S. S. A. Shah, T. Najam, M. Wen, S.-Q. Zang, A. Waseem, H.-L. Jiang, *Small Structures* **2022**, *3*, 2100090 (k) D. Yang, S. Zuo, H. Yang, Y. Zhou, Q. Lu, X. Wang, *Adv. Mater.* **2022**, *34*, 2107293 (l) Z. Di, Y. Qi, X. Yu, F. Hu, *Catalysts* **2022**, *12*, 1582 (m) Y.-L. Yang, Y.-R. Wang, L.-Z. Dong, Q. Li, L. Zhang, J. Zhou, S.-N. Sun, H.-M. Ding, Y. Chen, S.-L. Li, Y.-Q. Lan, *Adv. Mater.* **2022**, *34*, 2206706.

[35] H.-Q. Xu, J. Hu, D. Wang, Z. Li, Q. Zhang, Y. Luo, S.-H. Yu, H.-L. Jiang, *J. Am. Chem. Soc.* **2015**, *137*, 13440-13443.

[36] (a) K. S. Park, Z. Ni, A. P. Côté, J. Y. Choi, R. Huang, F. J. Uribe-Romo, H. K. Chae, M. O'Keeffe, O. M. Yaghi, *Proc. Natl. Acad. Sci.* **2006**, *103*, 10186-10191 (b) H. Hayashi, A. P. Côté, H. Furukawa, M. O'Keeffe, O. M. Yaghi, *Nat. Mater.* **2007**, *6*, 501-506 (c) R. Banerjee, A. Phan, B. Wang, C. Knobler, H. Furukawa, M. O'Keeffe, O. M. Yaghi, *Science* **2008**, *319*, 939-943 (d) Y. Wang, P. Hou, Z. Wang, P. Kang, *ChemPhysChem* **2017**, *18*, 3142-3147.

[37] (a) J. D. Evans, C. J. Sumby, C. J. Doonan, *Chem. Lett.* **2015**, *44*, 582-588 (b) T. Hasell, A. I. Cooper, *Nat. Rev. Mat.* **2016**, *1*, 16053 (c) H. H. Huang, T. Šolomek, *Chimia (Aarau)* **2021**, *75*, 285-290 (d) C. Chen, X. Yan, Y. Wu, S. Liu, X. Zhang, X. Sun, Q. Zhu, H. Wu, B. Han, *Angew. Chem. Int. Ed.* **2022**, *61*, e202202607 (e) G. Zhang, M. Mastalerz, *Chem. Soc. Rev.* **2014**, *43*, 1934-1947.

[38] (a) S. Hong, M. R. Rohman, J. Jia, Y. Kim, D. Moon, Y. Kim, Y. H. Ko, E. Lee, K. Kim, *Angew. Chem. Int. Ed.* **2015**, *54*, 13241-13244 (b) B. P. Benke, P. Aich, Y. Kim, K. L. Kim, M. R. Rohman, S. Hong, I.-C. Hwang, E. H. Lee, J. H. Roh, K. Kim, *J. Am. Chem. Soc.* **2017**, *139*, 7432-7435 (c) R. D. Mukhopadhyay, Y. Kim, J. Koo, K. Kim, *Acc. Chem. Res.* **2018**, *51*, 2730-2738 (d) Y. Kim, J. Koo, I.-C. Hwang, R. D. Mukhopadhyay, S. Hong, J. Yoo, A. A. Dar, I. Kim, D. Moon, T. J. Shin, Y. H. Ko, K. Kim, *J. Am. Chem. Soc.* **2018**, *140*, 14547-14551 (e) X. Yu, B. Wang, Y. Kim, J. Park, S. Ghosh, B. Dhara, R. D. Mukhopadhyay, J. Koo, I. Kim, S. Kim, I.-C. Hwang, S. Seki, D. M. Guldi, M.-H. Baik, K. Kim, *J. Am. Chem. Soc.* **2020**, *142*, 12596-12601 (f) J. Koo, I.

Kim, Y. Kim, D. Cho, I.-C. Hwang, R. D. Mukhopadhyay, H. Song, Y. H. Ko, A. Dhamija, H. Lee, W. Hwang, S. Kim, M.-H. Baik, K. Kim, *Chem* **2020**, *6*, 3374-3384.

[39] P. T. Smith, Y. Kim, B. P. Benke, K. Kim, C. J. Chang, *Angew. Chem. Int. Ed.* **2020**, *59*, 4902-4907.

[40] L. An, M. R. Narouz, P. T. Smith, P. De La Torre, C. J. Chang, *ChemRxiv* **2022**.

[41] P. T. Smith, B. P. Benke, L. An, Y. Kim, K. Kim, C. J. Chang, *ChemElectroChem* **2021**, *8*, 1653-1657.

[42] P. T. Smith, B. P. Benke, Z. Cao, Y. Kim, E. M. Nichols, K. Kim, C. J. Chang, *Angew. Chem. Int. Ed.* **2018**, *57*, 9684-9688.

[43] L. An, P. De La Torre, P. T. Smith, M. R. Narouz, C. J. Chang, *Angew. Chem. Int. Ed.* **2023**, *62*, e202209396.

[44] (a) M. Yoshizawa, M. Tamura, M. Fujita, *Science* **2006**, *312*, 251-254 (b) D. J. Tranchemontagne, Z. Ni, M. O'Keeffe, O. M. Yaghi, *Angew. Chem. Int. Ed.* **2008**, *47*, 5136-5147 (c) Z. Lu, C. B. Knobler, H. Furukawa, B. Wang, G. Liu, O. M. Yaghi, *J. Am. Chem. Soc.* **2009**, *131*, 12532-12533 (d) M. Yoshizawa, J. K. Klosterman, M. Fujita, *Angew. Chem. Int. Ed.* **2009**, *48*, 3418-3438 (e) Y. Inokuma, M. Kawano, M. Fujita, *Nat. Chem.* **2011**, *3*, 349-358 (f) R. Chakrabarty, P. S. Mukherjee, P. J. Stang, *Chem. Rev.* **2011**, *111*, 6810-6918 (g) T. R. Cook, P. J. Stang, *Chem. Rev.* **2015**, *115*, 7001-7045 (h) A. J. Gosselin, C. A. Rowland, E. D. Bloch, *Chem. Rev.* **2020**, *120*, 8987-9014 (i) C. E. Hauke, T. R. Cook, in *Comprehensive Coordination Chemistry III* (Eds.: E. C. Constable, G. Parkin, L. Que Jr), Elsevier, Oxford, **2021**, pp. 1074-1085 (j) C. T. McTernan, J. A. Davies, J. R. Nitschke, *Chem. Rev.* **2022**, *122*, 10393-10437 (k) J. Liu, Z. Wang, P. Cheng, M. J. Zaworotko, Y. Chen, Z. Zhang, *Nat. Rev. Chem.* **2022**, *6*, 339-356.

[45] (a) H. S. Lee, S. Jee, R. Kim, H.-T. Bui, B. Kim, J.-K. Kim, K. S. Park, W. Choi, W. Kim, K. M. Choi, *Energy Environ. Sci.* **2020**, *13*, 519-526 (b) X. Qi, R. Zhong, M. Chen, C. Sun, S. You, J. Gu, G. Shan, D. Cui, X. Wang, Z. Su, *ACS Catal.* **2021**, *11*, 7241-7248 (c) A. C. Ghosh, A. Legrand, R. Rajapaksha, G. A. Craig, C. Sassoye, G. Balázs, D. Farrusseng, S. Furukawa, J. Canivet, F. M. Wisser, *J. Am. Chem. Soc.* **2022**, *144*, 3626-3636.

[46] (a) M. Gong, Z. Cao, W. Liu, E. M. Nichols, P. T. Smith, J. S. Derrick, Y.-S. Liu, J. Liu, X. Wen, C. J. Chang, *ACS Cent. Sci* **2017**, *3*, 1032-1040 (b) A. Wagner, K. H. Ly, N. Heidary, I. Szabó, T. Földes, K. I. Assaf, S. J. Barrow, K. Sokołowski, M. Al-Hada, N. Kornienko, M. F. Kuehnel, E. Rosta, I. Zebger, W. M. Nau, O. A. Scherman, E. Reisner, *ACS Catal.* **2020**, *10*, 751-761.

Patricia De La Torre earned her B.S. in Chemistry in 2018 from Sonoma State University, where she worked with Dr. Carmen-Bustos Works on photo-induced structural changes in iron-iron hydrogenase model complexes. She is now an NSF Graduate Research Fellow

completing a PhD in Chemistry at the University of California, Berkeley with mentor Prof. Chris Chang. She has worked on molecular catalysis for electrochemical and photochemical carbon dioxide reduction.

Lun An completed his B.S. in Marine Chemistry from the Ocean University of China in 2013. He then pursued his graduate studies at the Shanghai Institute of Organic Chemistry with Prof. Xingang Zhang to work on transition-metal-catalyzed fluoroalkylation reactions and earned his Ph.D. in 2018. In 2019, he joined the laboratory of Prof. Chris Chang at the University of California, Berkeley as a postdoctoral associate to conduct energy catalysis research.

Christopher J. Chang is the Class of 1942 Chair Professor of Chemistry and Molecular and Cell Biology at the University of California, Berkeley, and Faculty Scientist at Lawrence Berkeley National Laboratory. Chris earned B.S./M.S. degrees from Caltech in 1997 and worked with Prof. Harry Gray, spent a year as a Fulbright scholar with Dr. Jean-Pierre Sauvage, and earned his Ph.D. from MIT in 2002 with Prof. Dan Nocera. After postdoctoral studies with Prof. Steve Lippard at MIT, Chris joined the Berkeley faculty in 2004. Research in the Chang laboratory focuses on the study of metals and redox-active molecules in biology and energy. They develop activity-based sensing and proteomics probes and catalysts to address questions in neuroscience, metabolism, and sustainable synthesis.

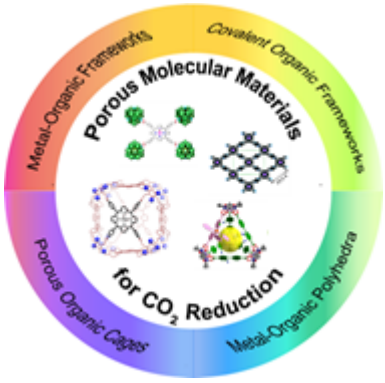

Table of contents: This mini-review showcases molecular materials catalysts for the CO_2 reduction reaction (CO_2RR) that feature permanent porosity as a design feature. Selected examples provide insights into how different approaches to this overall design strategy can augment their electrocatalytic and/or photocatalytic CO_2 reduction activity.

P. De La Torre, Dr. L. An, and Prof. C. J. Chang*

Porosity as a Design Element for Developing Catalytic Molecular Materials for Electrochemical and Photochemical Carbon Dioxide Reduction